Electronic Inhomogeneity in Correlated Materials

Steffen Wirth[#], M. Victoria Ale Crivillero, Hubert Dawczak-Dębicki, Jean C. Souza and Markus König

Electronic inhomogeneities are of great interest not only from a fundamental point of view but also for applications, e.g. in sensors and for spintronics. Here, we report on our research on two types of electronic inhomogeneity, namely nanoscale phase separation via the formation of magnetic polarons, and the formation of topologically non-trivial surface states. For the latter, we continued our efforts on the Kondo insulator SmB_6 by a systematic manipulation of its surface conductivity. For the half-Heusler compounds Y*T*Bi we showed that the impact of spin-orbit coupling on topology can be tuned by replacing T = Pd with Pt. Magnetic polaron formation was studied in depth for $Eu_5In_2Sb_6$, a material which exhibits colossal magnetoresistance. A possible nontrivial topology in this material remains elusive.

Materials in which the structural, electronic and magnetic degrees of freedom are entangled can exhibit unexpected or even spectacular physical phenomena like superconductivity, colossal magnetoresistance (CMR) or the Kondo effect [1, 2, 3]. A hallmark of such coupled degrees of freedom is the appearance of distinct electronic phases, often accompanied by phase separation and pattern formation. In this respect we continued two lines of research: i) topologically nontrivial surface states on different materials and ii) polaron formation in Eu-based compounds.

Over the past decade our primary experimental tool was low-temperature Scanning Tunneling Microscopy (STM) and Spectroscopy (STS). STM/S is perfectly suited to tackle the afore-mentioned topics because it combines atomic scale resolution with extreme surface sensitivity. Unfortunately, our most powerful STM equipment (base temperature of 0.3 K, ultra-high vacuum (UHV) conditions with *in situ* cleaving capabilities, magnetic field capability up to 12 T) broke down beyond repair. Since the implementation of a new UHV ^{3}He cryostat is only scheduled by the end of 2024, alternative experimental tools were established. One such technique is thermal expansion combined with magnetostriction measurements, implemented in our Physical Property Measurement System (PPMS). Its outstanding sensitivity and first results on tetragonal $DyRh_2Si_2$ and $HoRh_2Si_2$ have recently been reported [4, 5].

Topologically non-trivial materials

We continued our research on the topological Kondo insulator SmB_6 by a systematic manipulation of its surface conductivity [6, 7]. Albeit of topical interest, surprisingly little is known about the properties of the SmB_6 surface. In contrast to the bulk Sm valence of approximately +2.6 at low temperature, the valence at the surface appears to be closer to +3, which may be related to the formation of Sm_2O_3 near the surface. Moreover, despite the considerable stability of the bulk SmB_6 phase [8], the surface chemistry may be changed such that not only the chemical potential at the surface could be shifted, but also time-dependent surface properties may be observed. Consequently, if highly surface-sensitive techniques (like STM/S) are to be applied, clean SmB_6 surfaces are typically prepared by *in situ* cleaving in ultra-high vacuum (UHV) conditions. However, SmB_6 is difficult to break, and surfaces perpendicular to the main crystallographic axes of the cubic structure are polar in nature, very often giving rise to atomically rough or (2×1) reconstructed surfaces. Notably, even cleaved surfaces may exhibit valence inhomogeneities and band-bending effects, see [7]. But also for cases of less surface-sensitive techniques, like resistivity measurements, surfaces often need to be prepared, which may influence the surface itself, e.g. by disrupting the crystal structure at the surface, introducing impurities and subsurface cracks and/or, again, changing the Sm valence.

In order to investigate the surface conductance in a controlled and systematic way, we manipulated the sample

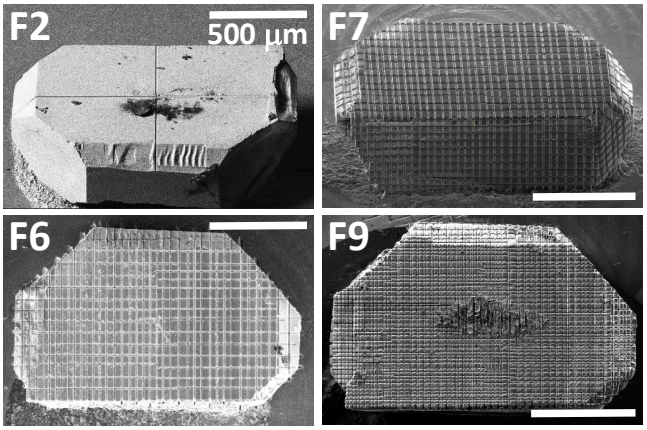

Fig. 1: SEM images of the same SmB_6 sample after cutting an increasing number of lines using a Focused Ion Beam (FIB) [6]. Shown are examples after FIB-runs F2, F6, F7 and F9. The dark patches at the centers of F2 and F9 are residue of paraffin used for fixing the sample. All scale bars: 500 µm.

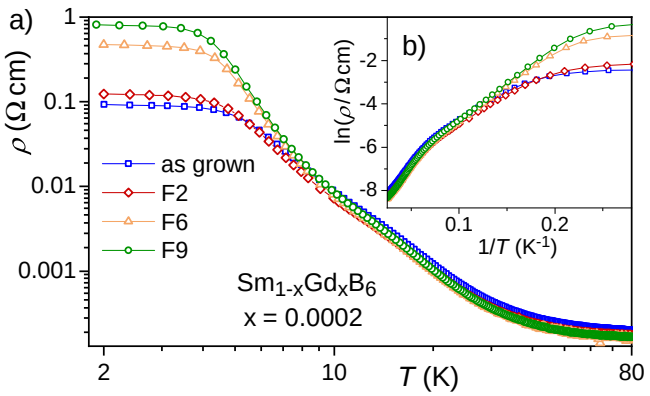

Fig. 2: (a) Double-logarithmic plot of the resistivity $\rho(T)$ of $Sm_{1-x}Gd_xB_6$ with $x = 0.0002$ before and after cutting an increasing number of lines by FIB (see Fig. 1). (b) $\ln\rho$ vs $1/T$ representation of the $\rho(T)$-data.

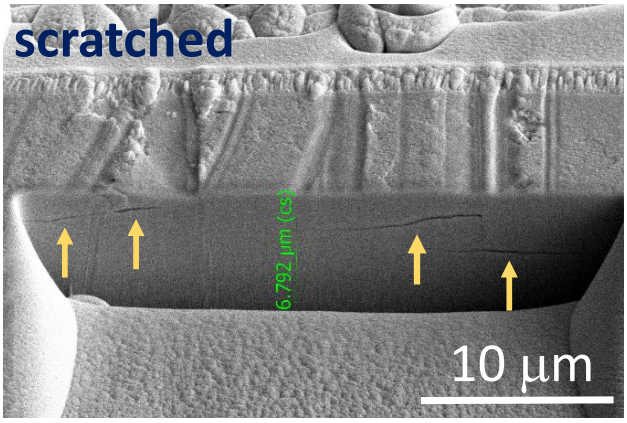

Fig. 3: Exemplary SEM image of a sample cross section underneath a scratched line. Cracks within the sample's bulk are clearly visible and marked by arrows.

surface utilizing a focused ion beam (FIB) [6]. Trenches of about 7–10 μm in depth were cut by Xe ions in consecutive runs, with each run about doubling the number of trenches cut. This results in ever smaller areas between the trenches, see Figure 1. For this example a minimum grid line distance of about 15 μm was achieved after the final run F9, which is still large compared to the effective carrier mean free path $\ell < 1$ μm [9]. Resistance measurements were conducted after some FIB runs, see Figure 2. Already the first cross of FIB-cut lines (F2) increases the $\rho(T)$-values within the plateau at low T compared to the as-grown surface by more than 30%, which appears to be well beyond the geometry inaccuracy. Upon increasing the FIB-cut line density, the low-T resistivity increases further such that $\rho(T)$ of F9 at lowest temperature exceeds the value of the as-grown surface by almost one order of magnitude. At the same time, the low-T limit within which thermally activated behavior is observed, drops by 2 K from as grown to F9, see Figure 2b. As expected, most other parameters remain largely unaffected by the FIB surface structuring. Consequently, the low-T surface conductivity can be tailored in a controlled fashion.

We investigated various samples of $Sm_{1-x}Gd_xB_6$ with $x = 0$ and 0.0002 without apparent difference. The small amount of Gd in one FIB-treated sample allowed for ESR, in addition to the successive resistance measurements for an increasing number of FIB cuts [9]. This provided further evidence for the contribution of surface or near-surface excitations to the relaxation mechanism in ESR due to nontrivial surface states.

Rough surface treatments can result in so-called subsurface cracks, Figure 3. In our example, these cracks were introduced by scratching the sample surface using a diamond scribe. Such subsurface cracks lower the value of the low-T resistance plateau by introducing additional conductance channels. This emphasizes that care must be taken when analyzing treated SmB_6 surfaces.

One of the most versatile class of compounds that host numerous topological states of matter is the half-Heusler compounds [10]. This family with a simple MgAgAs-type cubic structure has been extensively explored because they exhibit a plethora of different physical properties and hence, great potential for material design. Earlier theoretical calculations have suggested that the mechanism behind the appearance of topological features in this family depends on the band inversion, which is very similar to the one observed in the prototypical CdTe and HgTe systems and originates from the zinc blende crystal symmetry and strong spin-orbit coupling [11]. Consequently, comparing YPtBi and YPdBi can be an excellent platform to experimentally tune the topological properties through changes of the spin-orbit coupling as both systems possess very similar lattice parameters.

The challenge in using STM/S for comparison of the surface topology in YPtBi and YPdBi is related to the fact that *identical* surface terminations have to be investigated for both materials. Again, finding atomically flat surface areas on cubic half-Heuslers is extremely rare. In Figure 4a and 4d, YBi-terminated (120) surface planes of YPtBi and YPdBi, respectively, are shown [12]. As mentioned, YPtBi and YPdBi differ primarily in their spin-orbit coupling strength. Our STS results find the local density of states (DOS) to be finite at E_F for YPtBi, while the topologically trivial YPdBi compound exhibits a well-defined gap of ~100 meV around E_F, see Figure 4b and 4e, respectively. This clear difference is attributed to the presence of metallic surface states in YPtBi resulting from its non-trivial topology. Our band structure calculations, conducted specifically for the surface terminations as determined by STM beforehand, are consistent with such a change in the local DOS as shown in Figure 4c and 4f.

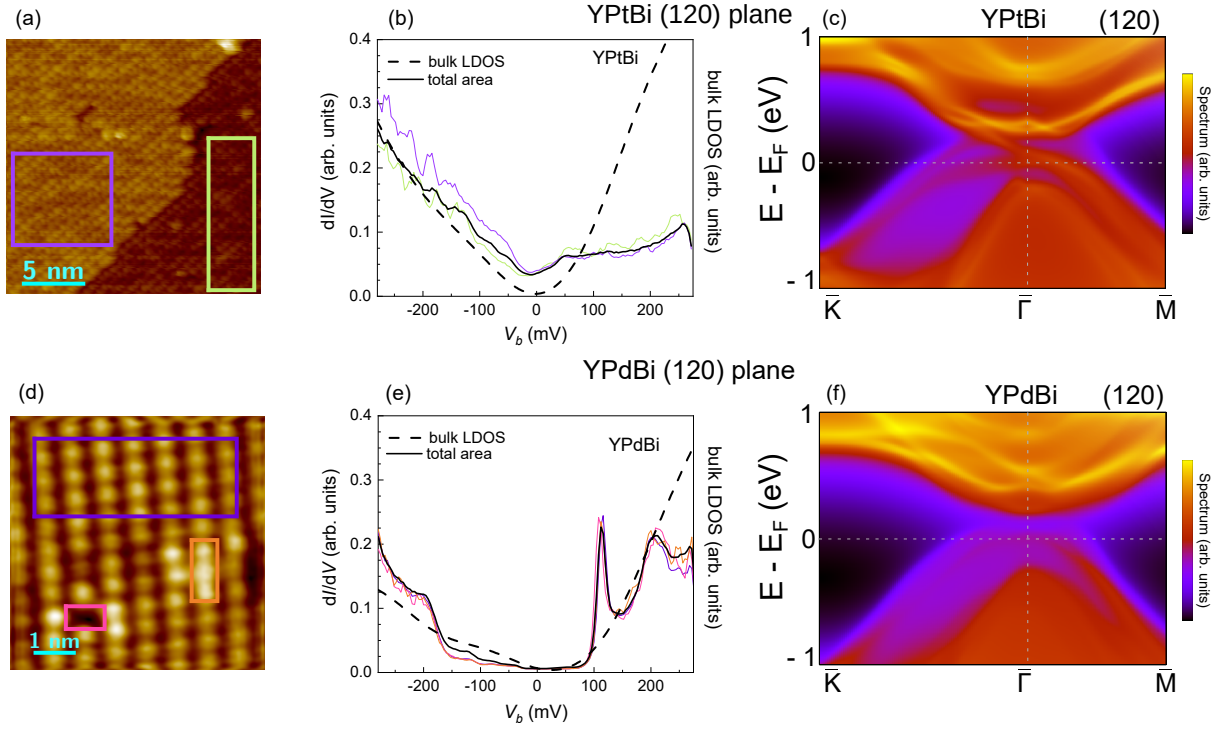

Fig. 4: (a) Atomically resolved topography of YPtBi (bias voltage $V_b = -200$ mV, $I_{sp} = 0.7$ nA, scale bar of 5 nm). Areas within which dI/dV-spectra were averaged are marked. (b) dI/dV-spectra within the purple and green rectangles as well as for the total area (black) presented in (a). Dashed line: calculated bulk DOS normalized at $V_b = -350$ mV to the experimental value. (c) Slab calculated electronic band structure for a YBi-terminated (120) surface of YPtBi clearly indicating spectral weight within the bulk gap near the Γ point. (d) 6×6 nm^2 topography for YPdBi ($V_b = -200$ mV, $I_{sp} = 0.6$ nA, scale bar of 1 nm). (e) dI/dV-spectra averaged over the magenta, orange, purple and the whole area shown in (d). Again, the calculated bulk DOS for YPdBi is included for comparison (dashed line). (f) Slab calculated electronic band structure for the YBi-terminated (120) plane of YPdBi.

Polaron formation in Eu-based compounds

CMR in the perovskites is typically accompanied by a mixed valence of Mn, double exchange and the presence of Jahn-Teller distortions [2]. The recent finding [13] of record CMR in the Zintl phase $Eu_5In_2Sb_6$ with pure Eu^{2+} has sparked a renewed interest in the mechanisms underlying the CMR effect.

We investigated $Eu_5In_2Sb_6$ by magnetic, electronic and specific heat measurements [14]. The complex structure of $Eu_5In_2Sb_6$ allows for three crystallographically different Eu sites and the Eu sublattices may magnetically order independently in which case the Dzyaloshinskii–Moriya interaction needs to be taken into consideration [15]. Despite the fact that Eu^{2+} ions have orbital angular momentum $L = 0$, there appear to be multiple, anisotropic exchange interactions in the magnetic and transport properties, compare Figure 5a and 5b. The inset of Figure 5a shows the ratio of resistivities measured at 9 T and 0 T from which an MR $= (\rho(9\,\mathrm{T}) - \rho(0\,\mathrm{T}))/\rho(0\,\mathrm{T})$ beyond −99.999% is found for $I \parallel a$. Most importantly, our thermodynamic and magnetotransport measurements along different crystallographic directions strongly indicate the formation of anisotropic polarons below about 130 K, i.e. well above the magnetic ordering temperatures T_{N1} and T_{N2} [14]. These polarons start to interact in the ab plane below about 30 K as clearly seen by a kink in $\rho(T)$, Figure 5a. In contrast, the resistivity $\rho(I \parallel c)$ in zero field continues to rise down to T_{N1}, i.e. without apparent interaction along the c direction. Application of a magnetic field supports the polaron formation regardless of the crystallographic direction and hence, the differences in $\rho(T)$ for $I \perp c$ and $I \parallel c$ abate, see inset to Figure 5b. We note that an oblate shape of the polarons with their short dimension along c is consistent with results from piezoresistance measurements [16].

Spin-resolved band structure calculations [15] suggested a spin configuration with ferromagnetically coupled Eu moments in the ab plane, which are alternatingly stacked in an antiparallel staggered order. Our angular dependent magnetization (M) measurements as well as the observation of a spin-flop transition in $M(H)$ for $H \parallel b$ indicate a preferred alignment of magnetic momentums along the b direction. According to the band structure calculations, the material has only rather few charge carriers available in the antiferromagnetic state and hence, it allows only

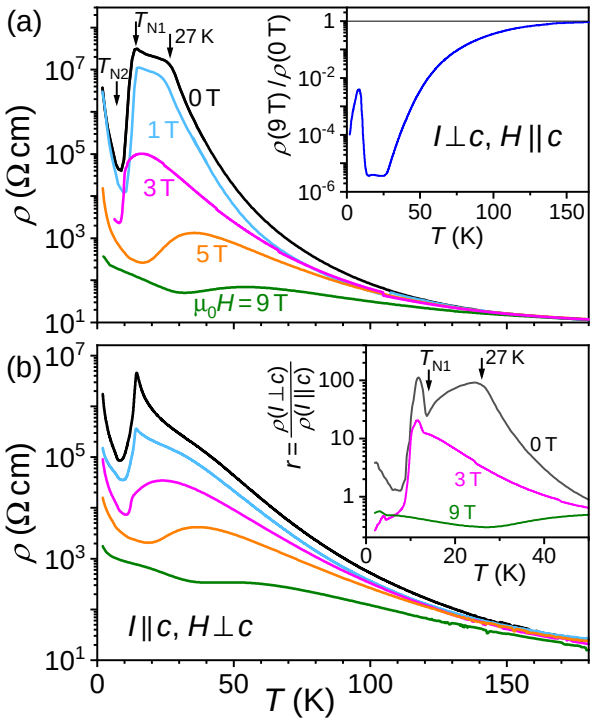

Fig. 5: Resistivity $\rho(T)$ in dependence on temperature for (a) current $I \parallel a$ and $H \parallel c$ as well as for (b) $I \parallel c$ and $H \parallel b$. Inset in (a) shows the ratio of resistivities $\rho(9\,\mathrm{T})/\rho(0\,\mathrm{T})$. The MR reaches beyond −99.999%. Inset in (b): Ratio r of resistivities for the different configurations presented in (a) and (b). The zero-field maximum near 27 K is suppressed with field. Panels share the same color code for magnetic fields.

for incoherent hopping transport via thermal activation. The former result is in good agreement with the very small but finite local DOS near E_F observed by STS on small patches of atomically flat surface areas, while the latter may lead to an effective insulator-like behavior as indeed observed in the resistivity measurements. Importantly, for a ferromagnetic spin configuration an enlarged DOS near E_F is predicted which illustrates how the difference in spin configuration can lead to a reorganization of the small band contributions near E_F and how interacting polarons can give rise to reduced resistivity.

In our earlier work [17], we established a procedure to directly visualize magnetic polarons in EuB_6 by utilizing Scanning Tunneling Spectroscopy (STS). However, a prerequisite for applying the procedure is atomically flat surfaces within areas much larger than the polaron size of typically a few nm. So far, our attempts to visualize magnetic polarons on $Eu_5In_2Sb_6$ by STS remain inconclusive because we could not, despite considerable effort, locate sufficiently large flat surface areas on *in situ* cleaved single crystals [15]. We also note that we were not able to confirm – neither experimentally nor theoretically – the existence of topologically nontrivial surface states [15]. The existence of such states has been speculated on the basis of the non-symmorphic space group *Pbma* the material $Eu_5In_2Sb_6$ crystalizes in, and the observation of topological order in the related compound $Ba_5In_2Sb_6$ [18].

External Cooperation Partners

Priscila F. S. Rosa (Los Alamos National Laboratory, Los Alamos, USA); Jens Müller, Kristin Kliemt, Cornelius Krellner (Goethe-University Frankfurt, Frankfurt (M), Germany); Ulrich K. Rößler (Institute for Solid State and Materials Research (IFW) Dresden, Germany); Stefan Schmult (Technical University Dresden, Germany); Pedro Schlottmann (Florida State University, Tallahassee, USA); Andrzej Ptok (Polish Academy of Sciences, Kraków, Poland); P. G. Pagliuso (Universidade Estadual de Campinas (UNICAMP), Campinas, Brazil).

References

[1] *From quantum matter to high-temperature superconductivity in copper oxides, B. Keimer, S. A. Kivelson, M. R. Norman, S. Uchida, and J. Zaanen, Nature* ***518*** *(2015) 179, https://dx.doi.org/https://doi.org/10.1038/nature14165*

[2] *Mixed-valence manganites, J. M. D. Coey, M. Viret, and S. von Molnár, Adv. Phys.****48*** *(1999) 167, https://dx.doi.org/https://doi.org/10.1080/000187399243455*

[3] *Exploring heavy fermions from macroscopic to microscopic length scales, S. Wirth, and F. Steglich, Nat. Rev. Mater.****1*** *(2016) 16051, https://dx.doi.org/https://doi.org/10.1038/natrevmats.2016.51*

[4]* *New applications for the world's smallest high-precision capacitance dilatometer and its stress-implementing counterpart, R. Küchler, R. Wawrzyńczak, H. Dawczak-Dębicki, J. Gooth, and S. Galeski, Rev. Sci. Instrum.****94*** *(2023) 045108, https://dx.doi.org/https://doi.org/10.1063/5.0141974*

[5]* *Coupling between magnetic and thermodynamic properties in RRh_2Si_2 (R = Dy, Ho), H. Dawczak-Dębicki, K. Kliemt, M. V. Ale Crivillero, R. Küchler, C. Krellner, O. Stockert, and S. Wirth, Phys. Rev. B* ***109*** *(2024) 134408, https://doi.org/10.1103/PhysRevB.109.134408, Editor's suggestion*

[6]* *Systematic manipulation of the surface conductivity of SmB_6, M. V. Ale Crivillero, M. König, J. C. Souza, P. G. Pagliuso, J. Sichelschmidt, P. F. S. Rosa, Z. Fisk, and S. Wirth, Phys. Rev. Research* ***3*** *(2021) 023162, https://dx.doi.org/https://doi.org/10.1103/PhysRevResearch.3.023162*

[7]* *An STM perspective on hexaborides: Surface states of the Kondo insulator SmB_6, S. Wirth, and P. Schlottmann, Adv. Quantum Technol.* ***4*** *(2021) 2100102, https://dx.doi.org/https://doi.org/10.1002/qute.202100102*

[8] *Phase stability in* SmB_6, *M. V. Ale Crivillero, S. Rößler, H. Borrmann, H. Dawczak-Dębicki, P. F. S. Rosa, Z. Fisk, and S. Wirth, Phys. Rev. Mater* ***5*** *(2021) 044204, https://dx.doi.org/https://10.1103/PhysRevMaterials.5.044204*

[9]* *Surface excitations relaxation in the Kondo insulator* $Sm_{1-x}Gd_xB_6$, *J. C. Souza, M. König, M. V. Ale Crivillero, M. O. Malcolms, R. R. Urbano, Z. Fisk, P. F. S. Rosa, P. G. Pagliuso, S. Wirth, and J. Sichelschmidt, Phys. Rev. Research* ***3*** *(2021) 033016, https://dx.doi.org/https://doi.org/10.1103/PhysRevResearch.3.033016*

[10] *Heusler, Weyl and Berry*, *K. Manna, Y. Sun, L. Muechler, J. Kübler, and C. Felser*, *Nat. Rev. Mater.****3*** *(2018) 244, https://doi.org/10.1038/s41578-018-0036-5*

[11] *Half-Heusler topological insulators: A first-principles study with the Tran-Blaha modified Becke-Johnson density functional, W. Feng, D. Xiao, Y. Zhang, and Y. Yao, Phys. Rev. B* ***82*** *(2010) 235121, https://link.aps.org/doi/10.1103/PhysRevB.82.235121*

[12]* *Tuning the topological character of half-Heusler systems: A comparative study on YTBi (T = Pd, Pt), J. C. Souza, M. V. Ale Crivillero, H. Dawczak-Dębicki, A. Ptok, P. G. Pagliuso, and S. Wirth, Phys. Rev. B* ***108*** *(2023) 165154, https://dx.doi.org/https://doi.org/10.1103/PhysRevB.108.165154*

[13] *Colossal magnetoresistance in a nonsymmorphic antiferromagnetic insulator, P. F. S. Rosa, Y. Xu, M. Rahn, J. Souza, S. Kushwaha, L. Veiga, A. Bombardi, S. Thomas, M. Janoschek, E. Bauer, M. Chan, Z. Wang, J. D. Thompson, N. Harrison, P. Pagliuso, A. Bernevig, and F. Ronning, npj Quantum Mater.* ***5*** *(2020) 52, https://dx.doi.org/https://doi.org/10.1038/s41535-020-00256-8*

[14]* *Magnetic and electronic properties unveil polaron formation in* $Eu_5In_2Sb_6$, *M. V. Ale Crivillero, S. Rößler, S. Granovsky, M. Doerr, M. S. Cook, P. F. S. Rosa, J. Müller, and S. Wirth, Sci. Rep.* ***13*** *(2023) 1597, https://dx.doi.org/https://doi.org/10.1038/s41598-023-28711-z*

[15]* *Surface and electronic structure at atomic length scales of the nonsymmorphic antiferromagnet* $Eu_5In_2Sb_6$, *M. V. Ale Crivillero, S. Rößler, P. F. S. Rosa, J. Müller, U. K. Rößler, and S. Wirth, Phys. Rev. B* ***106*** *(2022) 035124, https://dx.doi.org/https://doi.org/10.1103/PhysRevB.106.035124*

[16] *Colossal piezoresistance in narrow-gap* $Eu_5In_2Sb_6$, *S. Ghosh, C. Lane, F. Ronning, E. Bauer, J. D. Thompson, J. X. Zhu, P. F. S. Rosa, and S. M. Thomas, Phys. Rev. B* ***106*** *(2022) 045110, https://dx.doi.org/https://doi.org/10.1103/PhysRevB.106.045110*

[17] *Evidence for ferromagnetic clusters in the colossal-magnetoresistance material* EuB_6, *M. Pohlit, S. Rößler, Y. Ohno, H. Ohno, S. von Molnár, Z. Fisk, J. Müller, and S. Wirth, Phys. Rev. Lett.* ***120*** *(2018) 257201, https://dx.doi.org/https://doi.org/10.1103/PhysRevLett.120.257201*

[18] *Wallpaper fermions and the nonsymmorphic Dirac insulator, B. J. Wieder, B. Bradlyn, Z. Wang, J. Cano, Y. Kim, H.-S. D. Kim, A. M. Rappe, C. L. Kane, and B. A. Bernevig, Science* ***361*** *(2018) 246, https://dx.doi.org/https://doi.org/10.1126/science.aan2802*

[#]steffen.wirth@cpfs.mpg.de